ChemComm

COMMUNICATION

View Article Online
View Journal

Cite this: DOI: 10.1039/d4cc03511a

Received 14th July 2024,
Accepted 25th September 2024

DOI: 10.1039/d4cc03511a

rsc.li/chemcomm

Luminescent macroporous aerogels of two-dimensional nanocrystals of metal halide perovskites with adjustable semiconducting bandgaps†

Penghao Guo, Xuelian Jiang and Pei-Xi Wang *

In semiconducting aerogels, exciton–photon interactions occur in porous frameworks with solid–gas interfaces. Herein, by freezing and vacuum freeze-drying of cyclohexane dispersions of platelet-shaped nanocrystals of organic–inorganic metal halide perovskites, aerogels with macro-/meso-porosity, tunable luminescence in the visible light range, and photocurrent responses were fabricated.

As a class of solid materials with high specific surface areas, low bulk densities, and interconnected porosity, aerogels have been used in thermal insulation,[1] acoustic insulation,[2] batteries,[3] catalysis,[4] and many other fields. The combination of aerogels with luminescence or semiconductivity allows determination of the chemical properties and amounts of guest molecules or ions adsorbed in pores and channels, thus enabling applications in displays,[5] gas sensors,[6] pollution monitoring systems,[7] *etc.* Non-luminescent aerogels may acquire light-emitting features by incorporating fluorescent dyes,[8] quantum dots,[9] rare-earth elements,[10] or semiconducting nanoparticles.[11] Aerogels may also be fabricated from intrinsically luminescent microscopic building blocks such as Y_2O_3 nanosheets,[12] chalcogenides,[13] and CdSe/CdS nanocrystals.[14] To further extend the application range of luminescent aerogels, building blocks with broadly and precisely tunable emission wavelengths, high quantum yields, as well as high color purity would be necessary.

In recent years, layered hybrid organic–inorganic metal halide perovskites $(R\text{–}NH_3)_2MX_4$, a family of solution-processable ionic semiconductors that could be used in optoelectronics and light sources,[15] have attracted much attention due to their structural and compositional diversity.[16] By varying the interlayer organic ammonium cations ($R\text{–}NH_3^+$) as well as the divalent metal cations (M^{2+} = Pb^{2+}, Sn^{2+}, Mn^{2+}, *etc.*) and halide anions (X^- = Cl^-, Br^-, or I^-) at the centers and corners of MX_6^{2-} octahedral units, perovskites with different emission wavelengths ranging from near ultraviolet to near infrared may be synthesized.[17] In this research, perovskites were used as construction units of three-dimensional macro- and mesoporous frameworks, where by using cyclohexane (C_6H_{12}) that has a relatively high triple-point temperature of 279.47 K with a vapor pressure of 5.388 kPa,[18] colloidal dispersions of two-dimensional nanocrystals of layered metal halide perovskites were transformed into aerogels after freezing and vacuum freeze-drying. Semiconducting bandgaps of perovskite nanoplatelets were adjusted with the introduction of doping elements, thus enabling the fabrication of aerogels showing photoluminescence with blue, green, and red colors. Photocurrents of the perovskite aerogels were primarily tested under irradiation of ultraviolet and visible light, revealing tunable responsiveness to photons of different frequencies. These results suggest a new approach to aerogels with desired semiconducting bandgaps, and may guide the development of other semiconductive materials with porosity.

In our experiments, a two-dimensional lead(II) halide perovskite of bis(2-phenylethylammonium) tetrabromoplumbate(II) ($(C_6H_5\text{–}CH_2\text{–}CH_2\text{–}NH_3)_2PbBr_4$ was selected as the model material,[19] the crystals of which were synthesized by cooling a hot (373 K) clear aqueous solution containing hydrobromic acid (8.8 mol L^{-1}), lead(II) oxide (0.15 mol L^{-1}), and 2-phenylethylamine (0.30 mol L^{-1}) to 298 K over 2 hours. Colloidal nanoplatelets were prepared by slowly adding an *N*,*N*-dimethylformamide solution (0.30 mL) of $(C_6H_5\text{–}CH_2\text{–}CH_2\text{–}NH_3)_2PbBr_4$ (1.0 mol L^{-1}) into a chlorobenzene solution (10.0 mL, anhydrous) of *cis*-9-octadecenoic acid (0.1% by volume, 3.151 mmol L^{-1}) and *cis*-1-amino-9-octadecene (0.1% by volume, 3.039 mmol L^{-1}) at a stirring speed of 2400 revolutions per minute. About 10 minutes later, the reaction mixture was centrifuged at 9000 rpm for 10 minutes in a sealed centrifuge tube. The supernatant fluid was decanted, and the solids were redispersed in a cyclohexane solution (10.0 mL) of *cis*-9-octadecenoic acid and *cis*-1-amino-9-octadecene (0.3% by volume each) by sonication, then the dispersion was centrifuged again at 9000 rpm for 30 minutes to collect solids. This washing procedure was repeated two more times,

i-Lab, Suzhou Institute of Nano-Tech and Nano-Bionics of the Chinese Academy of Sciences, 398 Ruoshui Road, Suzhou, Jiangsu, 215123, P. R. China.
E-mail: pxwang2020@sinano.ac.cn

† Electronic supplementary information (ESI) available: Experimental methods and additional data. See DOI: https://doi.org/10.1039/d4cc03511a

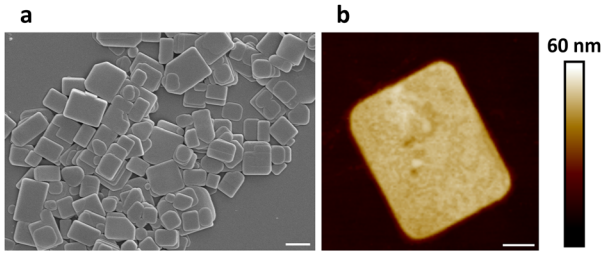

Fig. 1 SEM (a) and AFM (b) images of $(C_6H_5–CH_2–CH_2–NH_3)_2PbBr_4$ nanoplatelets. Scale bars: (a) 1 μm, (b) 200 nm.

and the solids were finally redispersed in 1.5 mL of the above-described cyclohexane solution to form a concentrated colloidal suspension. Under scanning electron microscopy (SEM) and atomic force microscopy (AFM), the colloids were observed to be rectangular-shaped two-dimensional nanocrystals with lengths of 500–2000 nm and thicknesses of 30–50 nm (Fig. 1a, b and Fig. S1, ESI†). The suspension was frozen in a glass vial (with an internal diameter of 16 mm) at about 77 K using liquid nitrogen, and lightweight aerogels were obtained after vacuum freeze-drying at a temperature of 193 K and a pressure of 5 pascals (Fig. 2a). In a typical experiment, a cylindrical aerogel of $(C_6H_5–CH_2–CH_2–NH_3)_2PbBr_4$ showed a diameter of 15.9 mm, a height of 6.8 mm, and a mass of 78.9 mg, corresponding to a macroscopic mass density of about 58.4 milligrams per square centimeter. Under ultraviolet light (wavelength of 365 nm), the aerogels exhibited blue-colored fluorescence (Fig. 2b), and photoluminescence spectroscopy (excitation wavelength at 365 nm) revealed a single emission peak at 413 nm (Fig. 3a).

By using an *N*,*N*-dimethylformamide solution (0.30 mL) of $(C_6H_5–CH_2–CH_2–NH_3)_2PbBr_4$ (1.0 mol L^{-1}) and manganese(II) bromide (0.2 mol L^{-1}) during the antisolvent-induced micro-precipitation process, colloidal nanoplatelets of manganese(II)-doped $(C_6H_5–CH_2–CH_2–NH_3)_2PbBr_4$ perovskites were synthesized (Fig. S2, ESI†). After liquid-nitrogen freezing at 77 K and

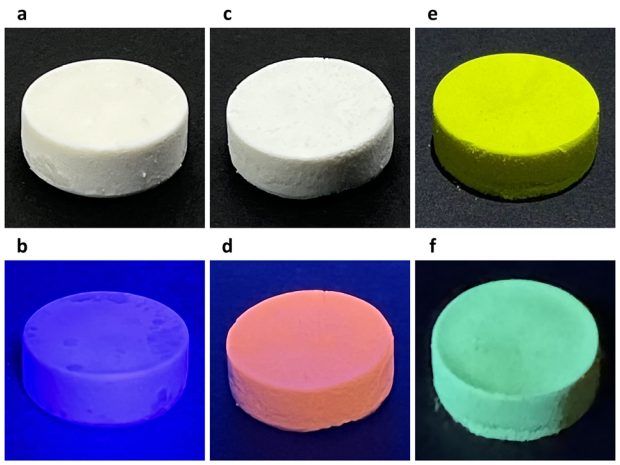

Fig. 2 Photographs of $(C_6H_5–CH_2–CH_2–NH_3)_2PbBr_4$ (a) and (b), $(C_6H_5–CH_2–CH_2–NH_3)_2Pb_{0.977}Mn_{0.023}Br_4$ (c) and (d), and $(C_6H_5–CH_2–CH_2–NH_3)_2PbBr_3I_1$ (e) and (f) aerogels under white (a), (c) and (e) and 365-nm ultraviolet light (b), (d) and (f). Diameters of the aerogels were 16 mm.

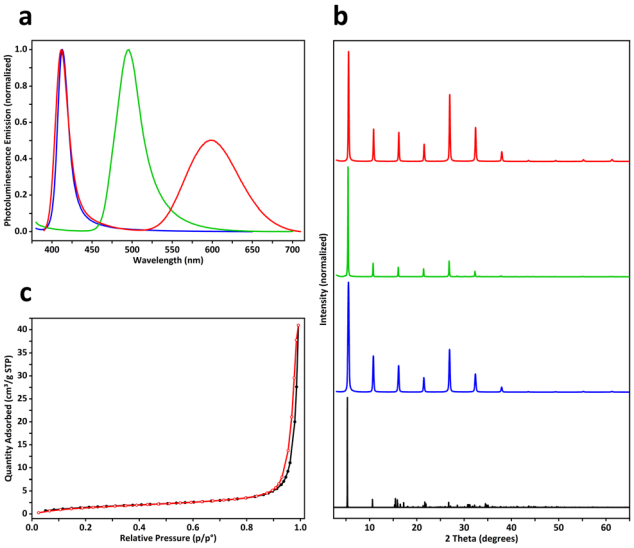

Fig. 3 (a) and (b) Emission spectra (a) and PXRD patterns (b) of $(C_6H_5–CH_2–CH_2–NH_3)_2PbBr_4$ (blue; simulated PXRD profile depicted in black), $(C_6H_5–CH_2–CH_2–NH_3)_2PbBr_3I_1$ (green), and $(C_6H_5–CH_2–CH_2–NH_3)_2Pb_{0.977}Mn_{0.023}Br_4$ (red) aerogels. (c) Nitrogen adsorption–desorption isotherms of $(C_6H_5–CH_2–CH_2–NH_3)_2PbBr_4$ aerogels.

vacuum freeze-drying, aerogels were fabricated (Fig. 2c), showing an actual doping concentration of 2.3 mol% manganese(II) as analyzed by inductively coupled plasma-optical emission spectroscopy (ICP-OES), a bulk mass density of about 113.3 mg cm^{-3}, red-colored fluorescence under 365-nm ultraviolet light (Fig. 2d), dual-band emission with two peaks at wavelengths of 412 nm and 598 nm (Fig. 3a), and a photoluminescence quantum yield of 2.6%, which was slightly higher than the 1.1% PLQY of aerogels formed by undoped $(C_6H_5–CH_2–CH_2–NH_3)_2PbBr_4$ nanoplatelets. By mixing $(C_6H_5–CH_2–CH_2–NH_3)_2PbBr_4$ (1.00 mol L^{-1}) and $(C_6H_5–CH_2–CH_2–NH_3)_2PbI_4$ (0.33 mol L^{-1}) in the DMF precursor solution (0.30 mL), $(C_6H_5–CH_2–CH_2–NH_3)_2PbBr_3I_1$ nanoplatelets (Fig. S3, ESI†) and aerogels were prepared (Fig. 2e), where the aerogels exhibited a macroscopic mass density of 66.7 mg cm^{-3}, green fluorescence under 365-nm light (Fig. 2f), a single emission peak at 496 nm (Fig. 3a), and a quantum yield of 10.5%. Powder X-ray diffraction patterns of fine powders of the above three perovskite aerogels revealed periodically spaced peaks matching those in simulated diffraction patterns calculated from the single-crystal X-ray crystallography data of $(C_6H_5–CH_2–CH_2–NH_3)_2PbBr_4$ (Fig. 3b).[20] In doped aerogels, Mn^{2+} and I^- were detected by X-ray photoelectron spectroscopy (Fig. S4, ESI†).

Nitrogen adsorption–desorption isotherms of a $(C_6H_5–CH_2–CH_2–NH_3)_2PbBr_4$ aerogel revealed a BET specific surface area of 5.83 $m^2\ g^{-1}$ and a BJH adsorption average pore width (4 V A^{-1}) of 42.5 nm (Fig. 3c), while BET specific surface areas of iodine- and manganese-doped perovskite aerogels were measured to be 1.87 and 4.46 $m^2\ g^{-1}$ (Fig. S5, ESI†), respectively. The relatively low surface areas may be caused by the large sizes of cyclohexane microcrystals.[21] Cross-sectional SEM images of $(C_6H_5–CH_2–CH_2–NH_3)_2PbBr_4$ aerogels showed hierarchical structures created by frozen and then sublimed cyclohexane microcrystals.

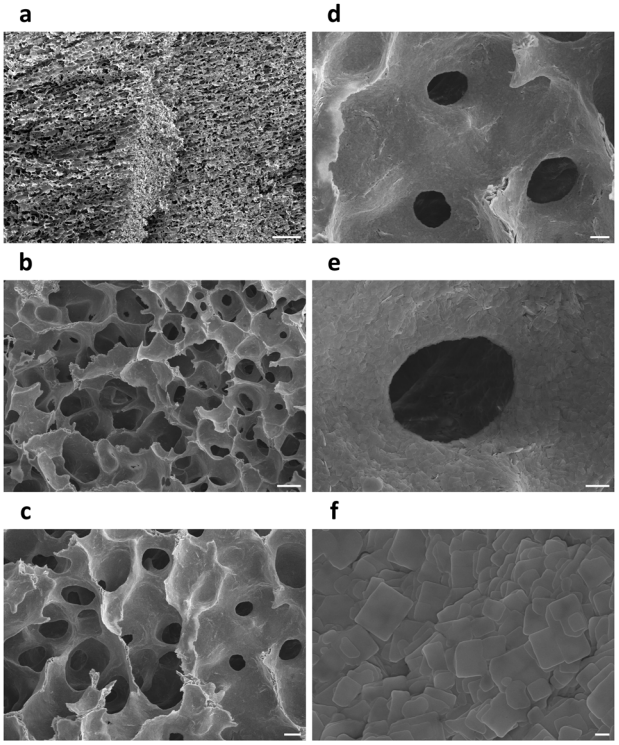

Fig. 4 Cross-sectional SEM images of a $(C_6H_5–CH_2–CH_2–NH_3)_2PbBr_4$ aerogel. Scale bars: (a) 200 μm, (b) 50 μm, (c) 20 μm, (d) 10 μm, (e) 4 μm, (f) 500 nm.

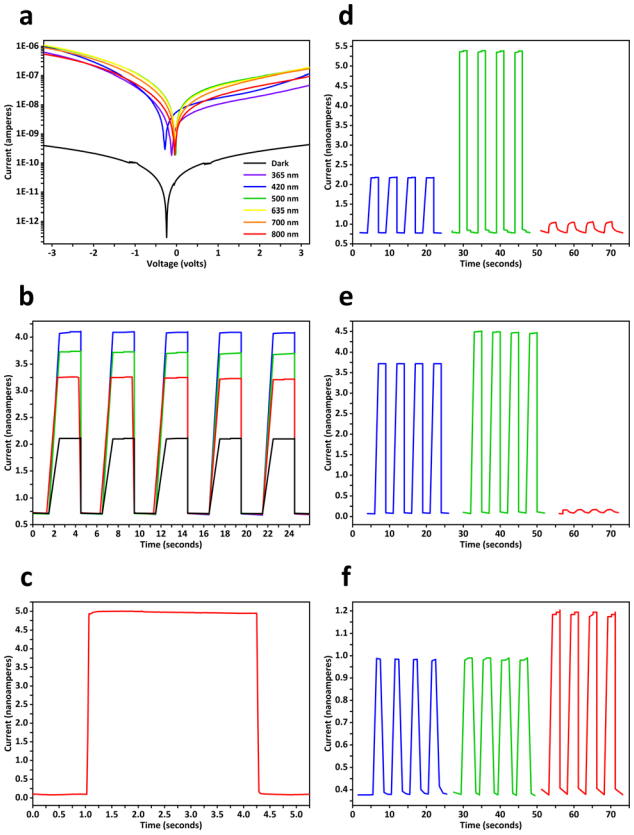

Fig. 5 (a) Current–voltage characteristics of a $(C_6H_5–CH_2–CH_2–NH_3)_2PbBr_4$ aerogel under 0.18 mW mm^{-2} illumination. (b) Time-resolved photocurrents of a $(C_6H_5–CH_2–CH_2–NH_3)_2PbBr_4$ aerogel under 365-nm irradiation with power densities of 0.18 (black), 0.35 (red), 0.50 (green), and 0.68 mW mm^{-2} (blue). (c) The rise and decay of the photocurrent in a $(C_6H_5–CH_2–CH_2–NH_3)_2PbBr_4$ aerogel during an on–off cycle of light (365-nm, 0.68 mW mm^{-2}). (d)–(f) Time-resolved photocurrents of $(C_6H_5–CH_2–CH_2–NH_3)_2PbBr_4$ (d), $(C_6H_5–CH_2–CH_2–NH_3)_2Pb_{0.977}Mn_{0.023}Br_4$ (e), and $(C_6H_5–CH_2–CH_2–NH_3)_2PbBr_3I_1$ (f) aerogels under 365-nm (blue), 420-nm (green), and 500-nm (red) lasers (0.18 mW mm^{-2}). From (b)–(f), a bias voltage of 1 volt was applied to the aerogels.

At low magnifications, parallel porous channels with millimeter-scale directional orderliness were observed (Fig. 4a), indicating local propagation directions of solidified cyclohexane during freezing. Frameworks of the aerogels were composed mainly of chamber-like macropores with diameters of 30–50 microns (Fig. 4b), and these chambers were further interconnected by micro-holes with widths of 5–20 μm (Fig. 4c and d). At higher magnifications, walls of the macropores were found to consist of aggregated perovskite nanoplatelets with rectangular geometry (Fig. 4e, f and Fig. S6, ESI†). Under SEM, aerogels of doped perovskites $(C_6H_5–CH_2–CH_2–NH_3)_2Pb_{0.977}Mn_{0.023}Br_4$ and $(C_6H_5–CH_2–CH_2–NH_3)_2PbBr_3I_1$ exhibited similar structures of unidirectionally ordered micro-channels and three-dimensional porous frameworks (Fig. S7 and S8, ESI†), suggesting that freezing and vacuum freeze-drying of colloidal cyclohexane dispersions of perovskites could efficiently transform them into aerogels.

Electrical and photoelectronic properties of the aerogels were evaluated by using transparent interdigitated electrodes made of indium tin oxide on glass, each of which had a digit length of 13 mm, a digit width of 0.2 mm, an inter-digit spacing distance of 0.2 mm, and 16 pairs of digits. Measurements of current–voltage characteristics were conducted in the dark and under illumination (0.18 mW mm^{-2}), where photocurrents of perovskite aerogels were approximately 1000 times higher than the corresponding dark currents (Fig. 5a and Fig. S9, ESI†). Time-resolved photocurrent responses of perovskite aerogels were examined under pulsed laser irradiation with different powers (Fig. 5b), revealing reproducible and abrupt on–off switching behaviors. During a typical off–on–off switch cycle, a $(C_6H_5–CH_2–CH_2–NH_3)_2PbBr_4$ aerogel showed rise and decay times (10–90%) less than 40 milliseconds (Fig. 5c). Responsivity of perovskite aerogels to photons of different wavelengths was dependent on their compositions. $(C_6H_5–CH_2–CH_2–NH_3)_2PbBr_3I_1$ aerogels with green emission and narrower energy bandgaps exhibited greater sensitivity to 500-nm light, and produced relatively higher photocurrents than those detected in undoped blue-emitting $(C_6H_5–CH_2–CH_2–NH_3)_2PbBr_4$ aerogels; while Mn^{2+} dopants may increase the density of charge carriers under 365-nm illumination (Fig. 5d–f).

In summary, semiconducting aerogels with macro-/meso-porosity and tunable luminescence were prepared by freezing and vacuum freeze-drying of nonpolar cyclohexane dispersions of colloidal two-dimensional nanoplatelets of layered organic–inorganic metal halide perovskites. Emission wavelengths of the aerogels were widely regulated by doping elements to achieve fluorescence with blue, green, and red colors. Photoelectronic analysis of perovskite aerogels under visible and

ultraviolet light revealed transient photocurrent responses and reproducible on–off switching behaviors. With porous spatial frameworks, high specific surface areas, and adjustable energy bandgaps, these hierarchically structured semiconductors may be used for gas sensing, catalysis, or long-distance diffuse illumination.

This research was supported by the National Natural Science Foundation of China (Young Scientists Fund 22205255), the Natural Science Foundation of Jiangsu Province (Young Scientists Fund BK20220297), the Youth Innovation Promotion Association of the Chinese Academy of Sciences (2023336), the Jiangsu Provincial Innovation and Entrepreneurship Talents Program (JSSCRC2022463; JSSCBS20211429), and the Gusu Innovation and Entrepreneurship Leading Talents Program (ZXL2022467).

Data availability

The data supporting this article have been included as part of the ESI.†

Conflicts of interest

There are no conflicts to declare.

Notes and references

1 S. S. Kistler and A. G. Caldwell, *Ind. Eng. Chem.*, 1934, **26**, 658–662.
2 P. P. Narang, *Appl. Acoust.*, 1991, **34**, 249–259.
3 D. B. Le, S. Passerini, A. L. Tipton, B. B. Owens and W. H. Smyrl, *J. Electrochem. Soc.*, 1995, **142**, L102–L103.
4 J. B. Miller, S. E. Rankin and E. I. Ko, *J. Catal.*, 1994, **148**, 673–682.
5 Z. He, X. Liang and W. Xiang, *Chem. Eng. J.*, 2022, **427**, 130964.
6 X. You, J. Wu and Y. Chi, *Anal. Chem.*, 2019, **91**, 5058–5066.
7 I. R. Pala and S. L. Brock, *ACS Appl. Mater. Interfaces*, 2012, **4**, 2160–2167.
8 N. Leventis, I. A. Elder, D. R. Rolison, M. L. Anderson and C. I. Merzbacher, *Chem. Mater.*, 1999, **11**, 2837–2845.
9 M. Zhang, J. Xue, Y. Zhu, C. Yao and D. Yang, *ACS Appl. Mater. Interfaces*, 2020, **12**, 22191–22199.
10 F. Liu, L. D. Carlos, R. A. S. Ferreira, J. Rocha, M. C. Gaudino, M. Robitzer and F. Quignard, *Biomacromolecules*, 2008, **9**, 1945–1950.
11 L. Sorensen, G. F. Strouse and A. E. Stiegman, *Adv. Mater.*, 2006, **18**, 1965–1967.
12 W. Cheng, F. Rechberger and M. Niederberger, *ACS Nano*, 2016, **10**, 2467–2475.
13 S. Bag, P. N. Trikalitis, P. J. Chupas, G. S. Armatas and M. G. Kanatzidis, *Science*, 2007, **317**, 490–493.
14 J. L. Mohanan and S. L. Brock, *J. Non-Cryst. Solids*, 2004, **350**, 1–8.
15 Y. Chen, Y. Sun, J. Peng, J. Tang, K. Zheng and Z. Liang, *Adv. Mater.*, 2018, **30**, 1703487.
16 L. Mao, C. C. Stoumpos and M. G. Kanatzidis, *J. Am. Chem. Soc.*, 2019, **141**, 1171–1190.
17 M. D. Smith, B. A. Connor and H. I. Karunadasa, *Chem. Rev.*, 2019, **119**, 3104–3139.
18 J. G. Aston, G. J. Szasz and H. L. Fink, *J. Am. Chem. Soc.*, 1943, **65**, 1135–1139.
19 D. Liang, Y. Peng, Y. Fu, M. J. Shearer, J. Zhang, J. Zhai, Y. Zhang, R. J. Hamers, T. L. Andrew and S. Jin, *ACS Nano*, 2016, **10**, 6897–6904.
20 K. Shibuya, M. Koshimizu, F. Nishikido, H. Saito and S. Kishimoto, *Acta Crystallogr., Sect. E: Struct. Rep. Online*, 2009, **65**, m1323–m1324.
21 D. C. Steytler, B. H. Robinson, J. Eastoe, K. Ibel, J. C. Dore and I. MacDonald, *Langmuir*, 1993, **9**, 903–911.

